

# Single electron detection and spectroscopy via relativistic cyclotron radiation

D. M. Asner,<sup>1</sup> R. F. Bradley,<sup>2</sup> L. de Viveiros,<sup>3</sup> P. J. Doe,<sup>4</sup> J. L. Fernandes,<sup>1</sup> M. Fertl,<sup>4</sup> E. C. Finn,<sup>1</sup>  
J. A. Formaggio,<sup>5</sup> D. Furse,<sup>5</sup> A. M. Jones,<sup>1</sup> J. N. Kofron,<sup>4</sup> B. H. LaRoque,<sup>3</sup> M. Leber,<sup>3</sup> E. L. McBride,<sup>4</sup>  
M. L. Miller,<sup>4</sup> P. Mohanmurthy,<sup>5</sup> B. Monreal,<sup>3</sup> N. S. Oblath,<sup>5</sup> R. G. H. Robertson,<sup>4</sup> L. J. Rosenberg,<sup>4</sup> G. Rybka,<sup>4</sup>  
D. Rysewyk,<sup>5</sup> M. G. Sternberg,<sup>4</sup> J. R. Tedeschi,<sup>1</sup> T. Thümmel,<sup>6</sup> B. A. VanDevender,<sup>1</sup> and N. L. Woods<sup>4</sup>

(Project 8 Collaboration)

<sup>1</sup>*Pacific Northwest National Laboratory, Richland, WA, USA*

<sup>2</sup>*National Radio Astronomy Observatory, Charlottesville, VA, USA*

<sup>3</sup>*Dept. of Physics, University of California, Santa Barbara, CA, USA*

<sup>4</sup>*Center for Experimental Nuclear Physics and Astrophysics, and  
Department of Physics, University of Washington, Seattle, WA, USA*

<sup>5</sup>*Laboratory for Nuclear Science, Massachusetts Institute of Technology, Cambridge, MA, USA*

<sup>6</sup>*Institut für Kernphysik, Karlsruher Institut für Technologie, Karlsruhe, Germany*

(Dated: Friday 13<sup>th</sup> May, 2022)

It has been understood since 1897 that accelerating charges must emit electromagnetic radiation. Cyclotron radiation, the particular form of radiation emitted by an electron orbiting in a magnetic field, was first derived in 1904. Despite the simplicity of this concept, and the enormous utility of electron spectroscopy in nuclear and particle physics, single-electron cyclotron radiation has never been observed directly. Here we demonstrate single-electron detection in a novel radiofrequency spectrometer. We observe the cyclotron radiation emitted by individual magnetically-trapped electrons that are produced with mildly-relativistic energies by a gaseous radioactive source. The relativistic shift in the cyclotron frequency permits a precise electron energy measurement. Precise beta electron spectroscopy from gaseous radiation sources is a key technique in modern efforts to measure the neutrino mass via the tritium decay endpoint, and this work demonstrates a fundamentally new approach to precision beta spectroscopy for future neutrino mass experiments.

For over a century, nuclear decay electron spectroscopy has played a pivotal role in the understanding of nuclear physics. Early measurements of the continuous  $\beta$ -decay spectrum [1] provided the first evidence of the existence of the weak force and the neutrino [2], and immediately hinted that the neutrino mass is small. Continuing this tradition, present efforts to directly measure the mass of the neutrino rely on precision spectroscopy of the  $\beta$ -decay energy spectrum of  ${}^3\text{H}$ . Because the value of the neutrino mass is an input to the Standard Model of particle physics as well as precision cosmology, a precision measurement of the neutrino mass would represent a significant advance in our description of nature.

The sensitivity of  ${}^3\text{H}$ -based neutrino mass measurements has been expanding over the past 80 years due to increasingly powerful electron spectrometry techniques. Prominent developments include electrostatic [3], magnetic [4], and electromagnetic [5, 6] techniques. The most sensitive limits to date place the neutrino mass below  $2\text{eV}/c^2$  [7–9]. A future experiment, the Karlsruhe TRITium Neutrino experiment (KATRIN) [10], is expected to be sensitive to masses an order of magnitude below this limit, but the lower bound, which neutrino oscillation measurements provide, is  $0.01\text{eV}/c^2$ .

A frequency-based technique has, in principle, the capability of overcoming the limitations imposed by traditional spectroscopic techniques. Since 1897, it has been known that accelerating charges emit electromagnetic radiation [11]. Cyclotron radiation, the particular form of radiation emitted by an electron orbiting in a magnetic field, was first derived in 1904 [12]; yet, single-

electron cyclotron radiation had never been observed directly. Here we demonstrate a technique for electron energy spectroscopy that directly measures the cyclotron radiation from single electrons. This technique, hereafter referred to as Cyclotron Radiation Emission Spectroscopy (CRES), could allow a future generation of experiments to access neutrino masses approaching or even reaching the oscillation bound [13].

Consider the ideal case where an electron is created in the presence of a uniform magnetic field  $B$ . The subsequent orbits of the electron have a cyclotron frequency  $f_\gamma$  that depends on the kinetic energy  $K$  of the electron:

$$f_\gamma \equiv \frac{f_c}{\gamma} = \frac{eB}{2\pi\gamma m_e}, \quad (1)$$

where  $e(m_e)$  is the electron charge (mass),  $c$  is the speed of light in vacuum, and  $\gamma = (1 + K/m_e c^2)$  is the Lorentz factor. The nonrelativistic frequency  $f_c$  is  $2.799\,249\,110(6) \times 10^{10}\text{ Hz}$  at 1 T [14]. The orbiting electron emits coherent electromagnetic radiation with a power spectrum that is strongly peaked at  $f_\gamma$ . Due to the  $K$  dependence of  $f_\gamma$ , a frequency measurement of this radiation is sensitive to the energy of the electron, and thus provides a new form of non-destructive spectroscopy.

In free space, the total radiated power  $P$  is given by the Larmor formula [15]:

$$P(\gamma, \theta) = \frac{1}{4\pi\epsilon_0} \frac{2}{3} \frac{e^4}{m_e^2 c^3} B^2 (\gamma^2 - 1) \sin^2 \theta, \quad (2)$$

where  $\epsilon_0$  is the permittivity of free space and  $\theta$  is the pitch angle of the electron, defined as the angle between the momentum vector of the electron and the direction of the magnetic field. For an electron with an energy near the 18.6 keV endpoint of  ${}^3\text{H}$ , approximately 1.2 fW is radiated in a 1 T magnetic field at a pitch angle of  $90^\circ$ .

The Project 8 collaboration has constructed an experiment designed to detect the cyclotron radiation from single electrons. At the heart of the experiment is a small volume hereafter referred to as the “cell”, in which the gaseous radioactive isotope  ${}^{83\text{m}}\text{Kr}$  is present at low pressure. The cell consists of a section of rectangular waveguide sized to capture the electron radiation and placed in a uniform static magnetic field. Electrons from  ${}^{83\text{m}}\text{Kr}$  decays are magnetically trapped inside the cell, where they emit cyclotron radiation. The cell waveguide is connected to the input of a low noise radio-frequency amplifier, where its output is digitized and analyzed offline as discussed below.

The radioactive isotope  ${}^{83\text{m}}\text{Kr}$  is a gamma-emitting isomer of  ${}^{83}\text{Kr}$  with a half-life of 1.8 h, in which internal conversion produces mono-energetic electron lines with kinetic energies of 17 830.0(5) eV, 30 227(1) eV, 30 424(1) eV, 30 477(1) eV and 31 942(1) eV, with line widths less than 3 eV [16]. The short-lived  ${}^{83\text{m}}\text{Kr}$  is supplied at a steady rate by decays of a 74 MBq source of the parent  ${}^{83}\text{Rb}$  with a half-life of 86 d, adsorbed onto zeolite beads [17]. As a noble gas, the krypton diffuses freely from the zeolite and uniformly fills the experimental system, including the cell, while non-evaporable getter pumps reduce the total pressure of non-noble gases to  $< 10 \mu\text{Pa}$ . The  ${}^{83\text{m}}\text{Kr}$  concentration and flow are monitored by means of a silicon detector that is exposed to the gas system but is outside the cell and magnet.

A magnetic field of near 1 T is provided by a 52 mm-diameter warm-bore superconducting solenoid magnet. To allow sufficient time for detection and precise measurement of the emission frequency, a weak magnetic trap is introduced at the midpoint of the cell to confine a small fraction of the produced electrons. A copper coil provides a near-harmonic magnetic field perturbation with a gradient of up to  $100 \text{ T m}^{-2}$  along the magnetic field axis and a maximum depth of  $-8.5 \text{ mT}$  at the trap’s center. With the strongest trap settings, an electron that is emitted with a pitch angle  $\gtrsim 85^\circ$  will be confined until collisions with the residual gas scatter the electron to a lower pitch angle.

The field strength inside the magnet bore is calibrated using both nuclear magnetic resonance (NMR) and electron spin resonance (ESR). A full NMR map of the magnetic field strength inside the bore of the magnet shows that the inhomogeneity of the background field near the center of the waveguide cell is negligible for the purposes of this measurement. ESR scans along the axis can be made with the waveguide in place by observing absorption of microwaves by a sample of 2,2-diphenyl-1-picrylhydrazyl (DPPH) inside a sealed Pyrex ampoule resting on the upper Kapton window of the cell. The field

strength at the center of the cell (without the additional trapping coil field) is measured to be  $0.9467(1) \text{ T}$ . Due to a slow drift in magnetic field and the effect of the trapping coil, the NMR and ESR measurements of the magnetic field were used only to predict the frequency region of interest and the achievable energy resolution.

At this field strength, the fundamental cyclotron signals for the 30.4 keV and 17.8 keV electrons are expected to lie in the microwave K band. Thus, the cell is constructed from a standard WR42 rectangular waveguide section ( $10.7 \times 4.3 \text{ mm}^2$ ) located at the center of the magnet bore, oriented with the longitudinal axis parallel to the solenoidal field. The  ${}^{83\text{m}}\text{Kr}$  source gas is confined to the 7.6 cm-long cell with 25  $\mu\text{m}$ -thick Kapton windows.

The motion of the electron in the cell couples strongly to the fundamental  $\text{TE}_{10}$  mode of WR42 waveguide, and most of the radiated power is emitted into this mode. The remainder of the power is coupled to higher order modes, which are non-propagating at the cyclotron frequency of the electron and are therefore unobservable to the receiver. The cell is coupled to a long waveguide that serves as the input to the receiver. The first stage of the receiver consists of two cascaded 22-40 GHz low noise preamplifiers that establish a noise floor of  $(20 \pm 5) \times 10^{-22} \text{ W Hz}^{-1}$ . The gain of this amplifier cascade is 54 dB, making the noise contribution from the components following these amplifiers negligible. The frequency band of interest (from 25 GHz to 27 GHz) is mixed down with a local 24.2 GHz oscillator to a center frequency of 1.8 GHz. A second mixer with a variable local oscillator frequency combines with a low-pass filter to select a frequency subband of 125 MHz for narrowband signal analysis. Signals are digitized at 250 MSPS with a free-running 8-bit digitizer and recorded to disk. A schematic of the receiver is shown in Figure 1.

The preamplifier performance is strongly dependent on physical temperature, which is reduced to 50 K by a Gifford-McMahon cryocooler. At that physical temperature, an equivalent noise temperature for the system may be derived by comparison with the available noise power from a matched resistor at temperature  $T_e$ , which is  $k_B T_e \text{ W Hz}^{-1}$ . Converting the amplifier noise floor to an available noise power, the noise temperature of the receiver is roughly 145 K. The expected signal-to-noise ratio (SNR) may be expressed as the ratio  $(E/k_B T_e)$  between the total energy radiated by the electron into the fundamental waveguide mode and the available noise power. For an 18 keV electron, the signal-to-noise ratio is 12 dB for a receiver detection bandwidth of 30 kHz.

The presence of a magnetic trapping field shifts the cyclotron frequency away from the purely homogeneous solution. Approximating the trap as harmonic, the primary signal frequency is

$$f(t) \simeq \frac{f_c}{\gamma} \left( 1 + \frac{\cos^2 \theta}{2 \sin^2 \theta} \right) \left( 1 + \frac{Pt}{\gamma m_e c^2} \right), \quad (3)$$

where it can be seen that electrons with pitch angles de-

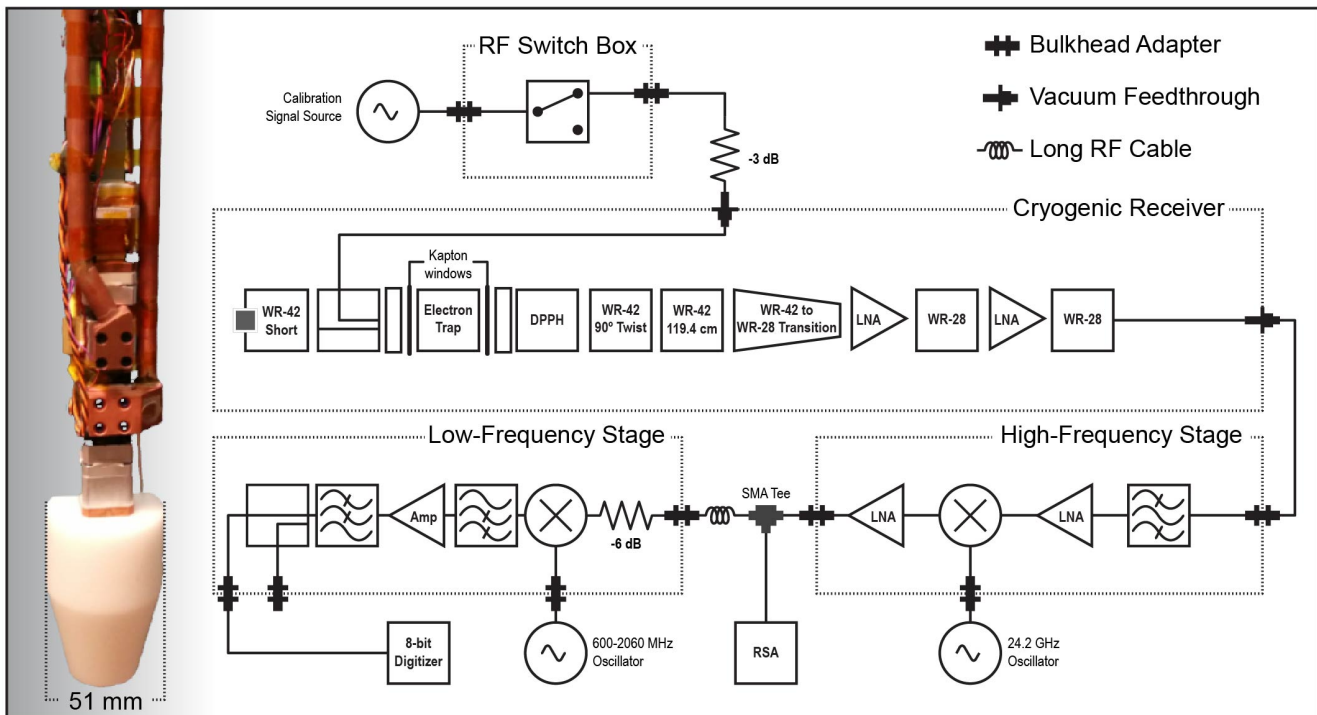


FIG. 1. A picture of the waveguide insert (left), where both the gas lines and trapping cell can be seen, and a corresponding schematic (right) of the receiver chain, consisting of cascaded cryogenic amplifiers, a high frequency stage and a low frequency stage. Calibrated radio frequency signals can be injected into the cryogenic receiver and through the WR42 waveguide section. The high frequency band of interest, with a width of 2 GHz centered at 26 GHz, is then mixed down to be centered at 1.8 GHz with the same 2 GHz bandwidth. A second amplification and mixing stage is used to further amplify the signal and shift the center frequency. Data can be recorded either using an 8-bit digitizer or through a real-time spectrum analyzer (RSA).

viating from  $\theta = 90^\circ$  emit cyclotron radiation at a higher frequency because they explore higher magnetic-field regions of the trap. As the electron radiates energy, the frequency will increase. Additional frequency structure is expected due to the axial and magnetron motion of the electron in the trap, but spectral lines due to this structure are relatively weak and have not yet been observed.

Equation 3 outlines the unique characteristics of a signal from a trapped electron. One expects to find a nearly-monochromatic RF signal at a frequency that slowly increases as the electron loses energy at a rate given by the Larmor formula. Electrons that scatter off the gas at small angles may remain confined and continue to radiate power at a frequency determined by the new pitch angle and the energy lost in the collision.

A Short Time Fourier Transform (STFT) with a window size of 8192 samples is performed on the digitized time series data to generate a spectrogram. The frequency and timing resolution of the transformed data is 30.52 kHz and 32.8  $\mu$ s; respectively. Bins in the spectrogram that exceed the noise floor by 8.12 dB are then extracted. The resulting reduced set of 2D data is examined for structures which appear linear in the time-frequency plane. Linear segments which are so discovered are then grouped in time into fully reconstructed electron

events. With the expected SNR, random alignments of power fluctuations should not occur.

The data show a large number of events with precisely the characteristics outlined above. Figure 2 shows the signal from a 30 keV electron observed during the first few milliseconds of data collection. The features expected for electron cyclotron emission are clearly evident, including (a) the abrupt onset of narrowband RF power above the surrounding background, (b) a quasi-linear increase in frequency over time as the particle loses energy via cyclotron emission and (c) sudden shifts in frequency due to gas collisions in which the electron remains magnetically confined. The power spectrum shown in Figure 2 is normalized to peak signal power. The absolute radiated power captured by the system for numerous subsequent electron events was also measured using the RSA as shown in Figure 1. The peak signal levels agreed with theoretical expectations. A clear excess of candidate events over background can be seen at 17.8 keV, 30 keV and 32 keV (see Figure 3). As a check for backgrounds, the excesses of candidate events are only observed when the magnetic trapping field is energized. The ratio of the peak frequencies, which is independent of the absolute magnetic field, is measured to be 1.023 870(60), in very good agreement with the expected weighted average peak

ratio of 1.023 875(2).

The energy resolution achievable with this technique depends on two factors: uncertainty in measuring the emission frequency, and uncertainty in the time at which the emission begins. Because of energy loss to radiation, the frequency is not constant but increases quasi-linearly with time. The achievable precision of a frequency measurement depends on the duration in which the signal is observed, usually terminated by the electron interacting with a gas atom. The precision in the time of onset has a fundamental quantum limit and a practical limit from thermal noise. The inherent resolution will be further broadened according to the sampled field inhomogeneity, and the latter is typically what dominates the overall energy resolution.

The uncertainty in the magnetic field from the DPPH measurement corresponds to an absolute energy uncertainty of 60 eV. Alternatively, one can use the 17.8 keV electron emission line to calibrate the mean field probed

by the trapped electrons, as has been done for Figure 3. This calibration method yields a relative uncertainty in the energy of about 30 eV and is currently limited by statistics as well as prior knowledge of the spectral line shape. A fit to the frequency distribution using a skewed gaussian line shape [18] yields a full width at half maximum of approximately 130 eV and 140 eV for the 17 keV and 30 keV emission lines; respectively. An apparatus designed to optimize resolution will be able to significantly decrease these uncertainties, which do not represent fundamental limits.

In summary, cyclotron radiation emission from single, mildly relativistic electrons has been observed experimentally. The observation renders frequency-based measurements of electron kinetic energy, with the advantages of precision and independence from nuclear and atomic standards, a practical approach. An important and immediate goal for CRES is the measurement of the mass of the neutrino.

- 
- [1] Chadwick, J. The intensity distribution in the magnetic spectrum of beta particles from radium (B + C). *Verh. Phys. Gesell.* **16**, 383–391 (1914).
- [2] Fermi, E. Tentativo di una teoria dei raggi  $\beta$ . *Ricerca Scient.* **2**, 12 (1933).
- [3] Hamilton, D. R., Alford, W. P. & Gross, L. Upper limits on the neutrino mass from the tritium beta spectrum. *Phys. Rev.* **92**, 1521–1525 (1953).
- [4] Bergkvist, K.-E. A high-luminosity, high-resolution study of the end-point behaviour of the tritium  $\beta$ -spectrum (ii). the end-point energy of the spectrum. comparison of the experimental axial-vector matrix element with predictions based on pcac. *Nuclear Physics B* **39**, 371 – 406 (1972).
- [5] Lobashev, V. & Spivak, P. A method for measuring the electron antineutrino rest mass. *Nuclear Instruments and Methods in Physics Research Section A: Accelerators, Spectrometers, Detectors and Associated Equipment* **240**, 305 – 310 (1985).
- [6] Picard, A. *et al.* A solenoid retarding spectrometer with high resolution and transmission for keV electrons. *Nuclear Instruments and Methods in Physics Research Section B: Beam Interactions with Materials and Atoms* **63**, 345 – 358 (1992).
- [7] Kraus, C. *et al.* Final results from phase II of the Mainz neutrino mass search in tritium beta decay. *Eur. Phys. J.* **C40**, 447–468 (2005).
- [8] Aseev, V. N. *et al.* Upper limit on the electron antineutrino mass from the troitsk experiment. *Phys. Rev. D* **84**, 112003 (2011).
- [9] Beringer, J. *et al.* Review of particle physics. *Phys. Rev. D* **86**, 010001 (2012).
- [10] Angrik, J. *et al.* KATRIN design report. *FZK Scientific Report 7090* (2005).
- [11] Larmor, J. A Dynamical Theory of the Electric and Luminiferous Medium. Part III. Relations with Material Media. *Royal Society of London Philosophical Transactions Series A* **190**, 205–300 (1897).
- [12] Heaviside, O. The Radiation from an Electron describing a Circular Orbit. *Nature (London)* **69**, 293–294 (1904).
- [13] Monreal, B. & Formaggio, J. A. Relativistic Cyclotron Radiation Detection of Tritium Decay Electrons as a New Technique for Measuring the Neutrino Mass. *Phys. Rev.* **D80**, 051301 (2009).
- [14] Mohr, P. J., Taylor, B. N. & Newell, D. B. Codata recommended values of the fundamental physical constants: 2010. *Rev. Mod. Phys.* **84**, 1527–1605 (2012).
- [15] Jackson, J. D. *Classical Electrodynamics* (Wiley; 3<sup>rd</sup> ed., 1998).
- [16] Picard, A. *et al.* Precision measurement of the conversion electron spectrum of  $^{83m}\text{Kr}$  with a solenoid retarding spectrometer. *Z. Phys.* **A342**, 71–78 (1992).
- [17] Venos, D., Spalek, A., Lebeda, O. & Fiser, M.  $^{83m}\text{Kr}$  radioactive source based on  $^{83}\text{Rb}$  trapped in cation-exchange paper or in zeolite. *Applied Radiation and Isotopes* **63**, 323–327 (2005).
- [18] L’Hoir, A. Study of the asymmetrical response of silicon surface barrier detectors to mev light ions. application to the precise analysis of light ions energy spectra i. helium ions. *Nuclear Instruments and Methods in Physics Research* **223**, 336 – 345 (1984).

## ACKNOWLEDGEMENTS

The Project 8 collaboration acknowledges financial support received from the University of Washington Royalty Research Foundation, the Massachusetts Institute of Technology Wade Fellowship, the U.S. Department of Energy Office of Science, Office of Nuclear Physics to the University of Washington under Award Number DE-FG02-97ER41020 and to the Massachusetts Institute of Technology under Award Number DE-SC0011091, the National Science Foundation under Award Number 1205100, and the Laboratory Directed Research and Development Program at Pacific Northwest National

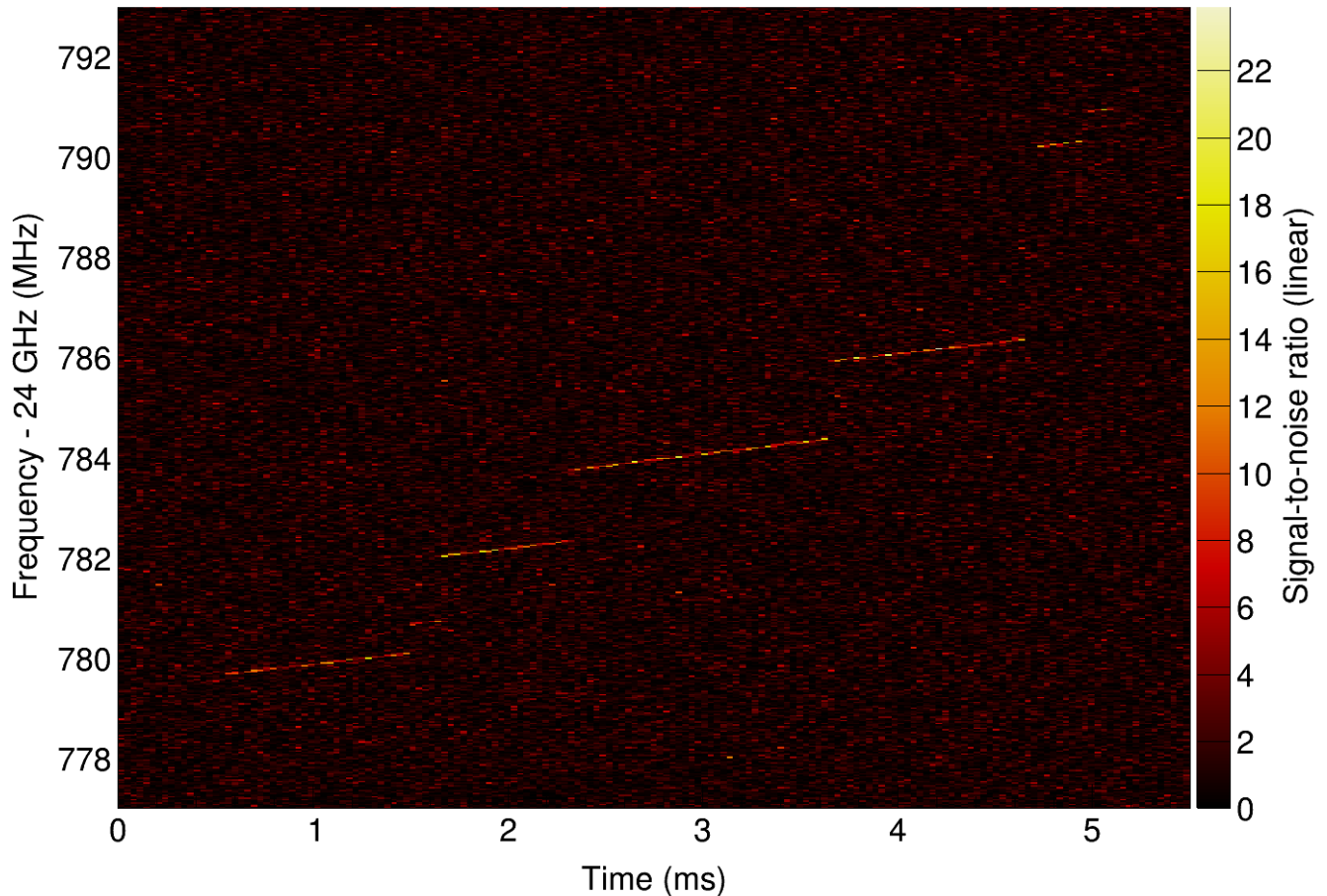


FIG. 2. A typical signal from the decay of  $^{83\text{m}}\text{Kr}$  characterized by an abrupt onset of narrowband power over the thermal noise of the system. The measured frequency reflects the kinetic energy of the electron, in this case 30 keV. The frequency increases slowly as the electron loses energy by emission of cyclotron radiation, ending in the first of six or possibly seven visible frequency jumps before the electron is ejected from the trap. The frequency-time window shown represents only a portion of an extended event lasting more than 15 ms. The sudden jumps result from the energy loss and pitch-angle changes caused by collisions with the residual gas, predominantly hydrogen. The most probable size of the energy jump, as determined from many events, is 14 eV.

Laboratory, a multiprogram national laboratory operated by Battelle for the U.S. Department of Energy under Contract DE-AC05-76RL01830. The Project 8 collaboration also wishes to thank: Dr. Otokar Dragoun and Dr. Drahoslav Venos for providing us with the zeolite for our source; Dr. Stefan Stoll for advice on ESR sources; and Dr. Jonathan Weintroub and Dr. Shep Doeleman for help with signal digitization development. A portion of the research was performed using PNNL Institutional Computing at Pacific Northwest National Laboratory.

#### AUTHOR CONTRIBUTIONS

Each of the authors participated in the collection and analysis of the data reported herein. According to the collaboration's publication policy, the authors are listed alphabetically.

#### COMPETING INTERESTS

The authors declare that they have no competing financial interests.

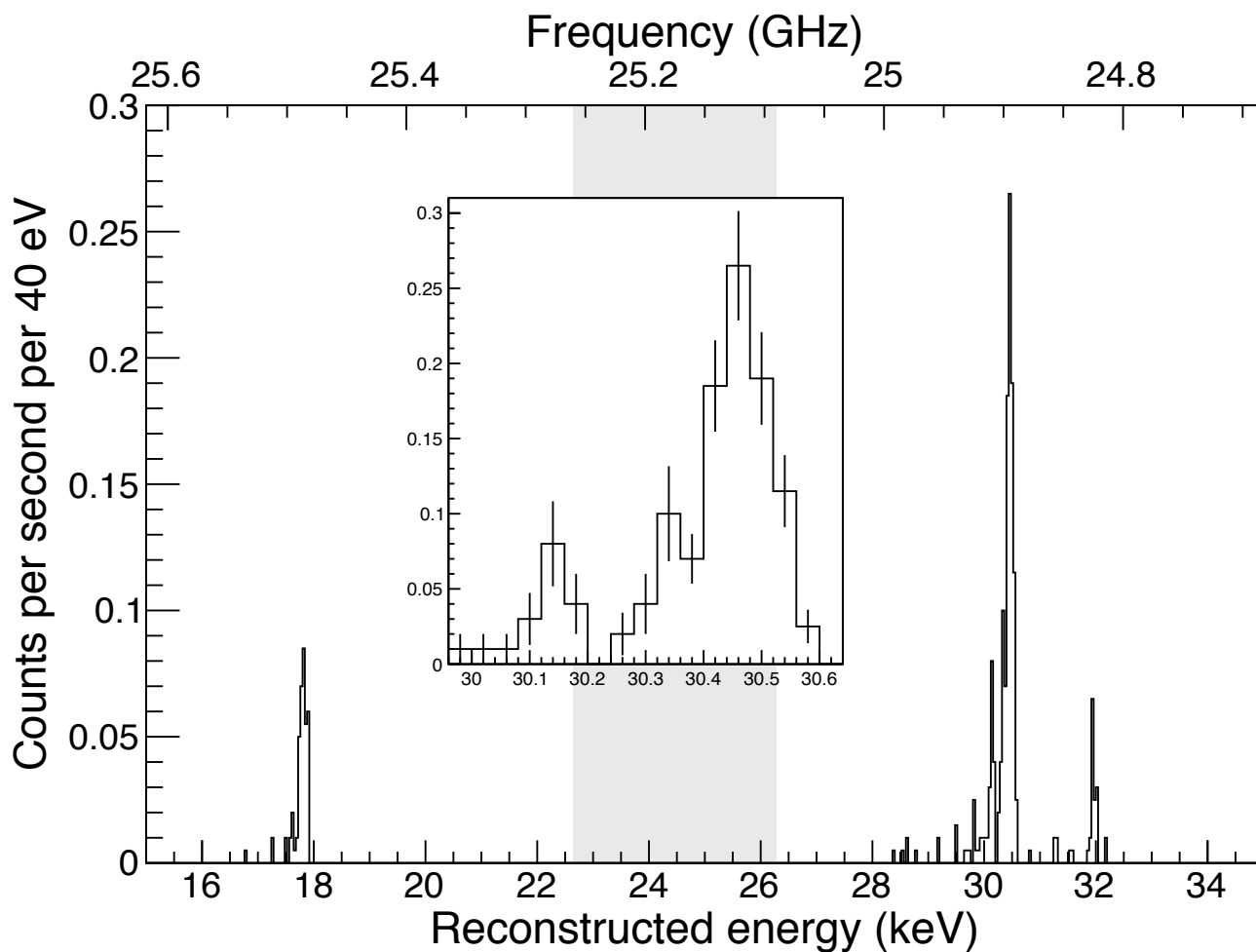


FIG. 3. The kinetic energy distribution of conversion electrons from  $^{83\text{m}}\text{Kr}$  as determined by CRES. The spectrum shows both the 17 keV, 32 keV and 30 keV-complex conversion electron lines. The shaded region indicates the bandwidth where no data were collected. Insert: An expanded view of the 30 keV energy region, where the 30.4 keV conversion electrons can be seen.

#### CORRESPONDENCE

Correspondence and requests for materials should be addressed to J. A. F. (email: josephf@mit.edu).